Cholinergic switch between two different types of slow waves in cerebral cortex

Trang-Anh E. Nghiem[1,2], Núria Tort-Colet[1,*], Tomasz Górski[1,2,*], Ulisse Ferrari[3], Shayan Moghimyfiroozabad[1], Jennifer S. Goldman[1,2], Bartosz Teleńczuk[1], Cristiano Capone[1,2,4], Thierry Bal[1], Matteo di Volo[1,2], and Alain Destexhe[1,2]

[1] Unité Neurosciences, Information et Complexité, Centre National de la Recherche Scientifique, Gif-sur-Yvette, France
[2] European Institute for Theoretical Neuroscience, Paris, France
[3] Sorbonne Université, INSERM, CNRS, Institut de la Vision, 17 rue Moreau, 75012 Paris, France
[4] Istituto Nazionale di Fisica Nucleare Sezione di Roma, Rome, Italy
*These authors contributed equally.
For correspondence: trang-anh.nghiem@cantab.net

Abstract. Sleep slow waves are known to participate in memory consolidation, but slow waves also occur in anesthetized states, with no positive effect on memory. Here, we shed light onto this paradox, based on a combination of analysis of extracellular recordings *in vitro* and in *in vivo* and computational models. We find two types of slow waves, based on analyzing the temporal patterns of successive slow-wave events. The first type of slow waves is seen during sleep, while the second type appears to prevail in anesthetized states. Network models of spiking neurons predict that these two slow-wave dynamics correspond to different levels of spike-frequency adaptation in excitatory cells. This prediction was tested *in vitro* by varying adaptation strength using an agonist of acetylcholine receptors, which demonstrated a neuromodulatory switch between the two types of slow waves. Finally, we show that the first type of slow-wave dynamics is more sensitive to external stimuli, which can explain how slow waves in sleep and anesthesia differentially affect memory consolidation, as well as provide a link between slow-wave dynamics and memory diseases.

Significance statement. During sleep, cortical neurons display slow oscillations, which are believed to participate in memory consolidation. However, it remains unknown why the apparently similar slow-wave dynamics seen under anesthesia do not produce the same effect on memory. Here, we show distinctive features of slow oscillatory patterns in sleep versus anesthesia, robust across species and anesthetics. Using computational modeling and in vitro preparations, we show that in anesthesia, depressed neuromodulation stabilizes neural dynamics, limits communication between neural assemblies, and can explain why memory encoding is prevented. Because the same neuromodulatory system is depressed in both anesthesia and Alzheimers disease, our results offer a mechanistic link between the sleep and memory symptoms of the disease, with implications for the identification of novel therapeutics.

1 Introduction

In both natural sleep and anesthesia, cortical dynamics are characterized by slow, irregular oscillations (<1 Hz) [1]. However, certain cognitive processes, such as those involved in memory formation [2–4], are specific to deep sleep (also known as Slow-Wave Sleep, SWS), but not to anesthesia. While contrasts between sleep and anesthesia are relatively well-studied at the whole-brain scale [5–7], any underlying differences in the microscopic dynamics of cortical neural networks and their potential mechanisms remain to be identified. In fact, while anesthesia and sleep appear to produce similar collective dynamics, it it still unknown whether any differences exist in the correlation structure of network dynamics between the two states, and how they may affect the system's ability to encode and remember stimuli.

At the neural population level, in both sleep and anesthesia, slow oscillations emerge from the alternation between transients of high neural firing (UP states) and transients of near silence (DOWN states) [1]. While certain regimes of anesthesia present very regular UP and DOWN states [8–10], in obvious contrast with the irregular patterns observed during sleep slow waves [7], irregular regimes also exist under anesthesia [10–12], and appear to present more 'sleep-like' dynamics. Additionally, UP-DOWN state activity has also been obtained in slice preparations *in vitro* [13]. Due to their general similarity in collective dynamics, slices and anesthesia, where direct pharmacological manipulation is possible, have often been used as models of natural sleep, paving the way to investigating mechanisms underlying UP-DOWN state activity.

Nevertheless, sleep and anesthesia present different levels of neuromodulation, known to affect the electrophysiological properties of neurons and how they respond to external inputs. In particular, as anesthesia is characterized by lower concentrations of acetylcholine (ACh) compared to sleep [14, 15], the net effect is an enhancement of spike-frequency adaptation driven by K^+ channels [16]. Following the increasing electrophysiological detail available on single neuron dynamics, computational models of spiking neurons have been employed to model spike-frequency adaptation and account for UP-DOWN state dynamics [17–19]. Indeed, comparison of models with neural recordings in anesthesia has recently uncovered a mechanistic interpretation for the emergence of UP and DOWN states, where background noise and neuromodulation, which controls spike-frequency adaptation, can account for the transitions between UP states and DOWN states [11]. While background noise is able to trigger a transition from a DOWN to UP state, spike-frequency adaptation on excitatory cells produces a self-inhibition that, destabilizing the UP state, causes a reset to the DOWN state [18]. However, it is plausible that subtle mechanistic particularities at the microscopic scale could be expressed as differences in the collective network dynamics that underlie distinct computational properties of sleep and anesthesia.

In the present paper, we find fundamental differences in correlation structure in slow waves during sleep and anesthesia, that can explain the different capacity for information encoding between the two states. We investigate computational

models to search for plausible mechanisms underlying these differences. These mechanisms will be subsequently tested in *in vitro* preparations displaying UP-DOWN state dynamics, and where pharmacological manipulation is possible. In sum, we will show in which ways slow-wave dynamics differ between anesthesia and slow-wave sleep, robustly across different anesthetics, brain regions, and species, and propose possible mechanisms and functional consequences of these differences.

2 Results

To compare with previous anesthesia results [10, 11], we consider the activity of a population of 10^2 neurons recorded from the temporal cortex of a human patient (Fig. S1A-C) during sleep. The dynamics is characterized by slow waves, as evident from Local Field Potentials (LFP) associated with an alternation of low (DOWN) and high (UP) activity periods, as visible in spiking activity. In all our analyses UP and DOWN states are defined based on neuron spiking activity (see Supplementary Materials and Methods). The time duration of both DOWN and UP states are variable, following an exponential, long-tailed distribution (see Supplementary Materials and Methods), similar to what has been reported for anesthesia recordings [11].

While the distributions of UP and DOWN state durations found in sleep and anesthesia are similar, surprisingly, the temporal distribution of UP and DOWN state durations is different in sleep compared to anesthesia. In anesthesia, DOWN state and next UP state durations are positively correlated, in other words long DOWN states are followed by long UP states, as shown in previous work [11]. However, we find that in sleep, DOWN state and next UP state durations are negatively correlated, as long DOWN states are followed by short UP states (Fig. 1B). Indeed, during sleep, while long UP states can occur after short DOWN states, UP states following long DOWN states are consistently short.

Because a difference in temporal correlation was found for adjacent UP and DOWN epochs between sleep and anesthesia, we next explored whether the network retains a memory of previous epochs further in time. To this end, correlations between the n-th DOWN state and the (n+k)-th UP state duration were explored. Here, $k = 0$ denotes the UP state following the nth DOWN state, as studied so far, while $k = -1$ denotes the UP state preceding the nth DOWN state in time. As shown in Fig.1C, the length of time correlations remain between DOWN and UP states lag k remains significantly negative up to a separation on the order of five UP/DOWN cycles in sleep data. In contrast, the correlations at lag k decay to zero immediately after one UP/DOWN state cycle in anesthesia [11]. Thus, the network retains a memory of previous cycles significantly longer in SWS than anesthesia.

In order to investigate whether the correlation between UP-DOWN state duration and its memory through time are specific to brain states across species and regions of cortex, data from primary visual cortex of animals under different anesthetics (monkey under sufentanil, rat under ketamine and medetomidine),

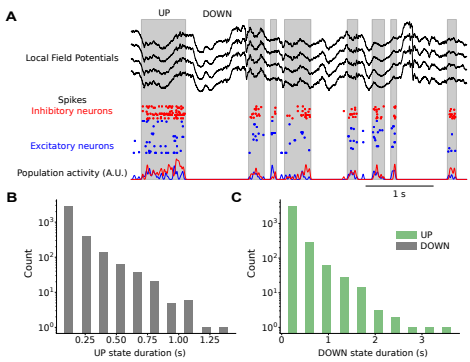

Fig. 1. Different types of slow waves during sleep and anesthesia, across species, brain regions and anesthetics. (A) LFP (top panel) and spiking data (bottom) recorded by multi-electrode array implanted into a human patient's temporal cortex. Slow oscillations (¡1 Hz) visible in the LFP correspond to an alternation between transients of high and low firing rate, i.e. UP and DOWN state dynamics, evident in the spiking activity (grayed: UP state detection based on population spike count, see Supplementary Materials and Methods). (B) UP state duration against previous DOWN state duration, showing a clear negative correlation. (C) Bar plot of Pearson correlation $C(D_{n+k}, U_n)$ as a function of lag k. Two standard deviations of the Pearson correlations when shuffling state durations (dashed lines) provide an interval of confidence outside of which empirical correlations may be considered non-trivial. The same analyses is reported for other species during sleep and anesthesia: sleep in the monkey premotor cortex (D) and in the rat pre-frontal cortex (E), anesthesia in the monkey (G) and rat V1 (H). Panels (F) and (I) report the lag-correlation during sleep and anesthesia in the rat.

and several animals sleeping (human temporal cortex, monkey premotor cortex, and rat prefrontal cortex) was analyzed.

The results of these analyses are reported in Fig.1 where in panels D-I we show the scatter plot of DOWN against following UP state duration. In all the sleep recordings a banana-shaped distribution is observed, indicating a robust negative UP-DOWN state correlation (for sleeping rats, 5/5 of animals analyzed showed a negative correlation, both before and after a navigation task).

Conversely, in anesthetized recordings the results are consistent with previously published results [11], an either positive or non-significant correlation is recorded (for anesthetized monkeys, 5/6 recordings presented a significant correlation and 1/6 a non-significant correlation; for anesthetized rats, 4/7 animals showed a significant positive correlation, 2/7 showed a positive non-significant correlation and the remaining 1/7 showed a negative significant correlation.)

Moreover, comparing within the same species (Fig.1F, I), the lag-correlation is verified to be different between sleep and anesthesia (we compare here the same species for the sake of coherence), with a much longer memory during sleep.

These observations suggest a clear difference in the correlation structure of the network dynamics during sleep and anesthesia, revealing fundamental differences in the dynamical mechanisms determining UP-DOWN state activity.

Spiking network model of UP and DOWN state dynamics

In order to investigate the mechanisms behind the UP and DOWN state duration correlations, we use a network of spiking neurons with conductance-based (COBA) synapses. The network is composed of 80% RS (regular spiking) excitatory and 20% fast spiking (FS) inhibitory neurons. Every neuron is modeled as an Adaptive Exponential integrate-and-fire cell (AdExp) [20]. In absence of adaptation the system is characterized by two stable states: a near-silent state (DOWN state) and a relatively high-activity state (UP state).

To allow for transitions between the two states, every neuron receives an independent identically distributed (i.i.d.) zero-mean noise of amplitude σ that permits a jump from the DOWN to the UP state. The presence of spike-frequency adaptation of strength b (see Supplementary Materials and Methods) for RS neurons [21] allows the system to transition back to the DOWN state. Indeed, RS neuron adaptation builds up as the neuron spikes, i.e. during UP states, and consequently reduces the firing rate of the excitatory population, which may cause the transition to a DOWN state. Adaptation decays exponentially throughout time when the neuron is silent, for instance during DOWN states (see Supplementary Materials and Methods for equations).

Such mechanisms for the emergence of UP and DOWN state dynamics has been so far established in the literature (see e.g. [11, 22]). We observed the same mechanism in a spiking network model of Adaptive integrate and fire neurons with voltage-dependent synapses and a different gain between excitatory and inhibitory cells following experimental insights (see Supplementary Materials and Methods). The network dynamics is characterised by an alternation between UP and DOWN states whose durations follow an exponential distribution, in accordance with experimental data (see Fig 1C for data and Supplementary material for the model). For a fixed value of noise amplitude σ we observe a positive correlation between UP-DOWN dynamics, where the adaptation strength b changes the UP-DOWN duration, with no obvious effect on their correlation. The correlation between UP and DOWN state duration remains positive or non-significant over the all range of b values here investigated. This is consistent with adaptation having decayed after long DOWN states: following noise-triggered onset, the following UP state displays a high rate of activity that may sustain a long UP state. Consequently, long DOWN states tend to be followed by long UP states, hence the positive correlation. Exploring the parameter space by varying other parameters such as neurons' excitability or synapses' quantal conductances, positive or non-significant correlations were also always obtained.

In accordance with previously reported results [11], the model discussed so far is suitable for UP-DOWN dynamics during anesthesia but not for sleep, where we have shown a clear and robust inverse relationship. This shows addi-

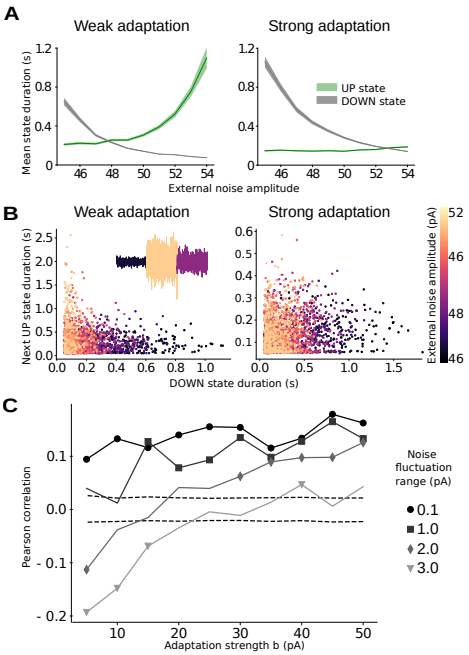

Fig. 2. Interplay between spike-frequency adaptation strength and noise amplitude allows for a transition from sleep-like to anesthesia-like slow waves in a spiking network model. UP and DOWN state duration vs amplitude of external noise, for low (A) and high (B) adaptation strength in the spiking network model (see text and Supplementary Materials and Methods). (B) UP state duration against previous DOWN state duration for external noise amplitude varying throughout time (see the inset for noise time course) in the range $[-\Delta, \Delta]$. Here, $\Delta = 3$ pA, showing a negatively correlated (r = -0.15, p ¡¡ 0.001), 'sleep-like' durations for low adaptation (left) and uncorrelated (r = -0.01, p ¿¿ 0.05), 'anesthesia-like' correlations for high adaptation (right). (C) Variation of next UP to previous DOWN state correlation as a function of adaptation strength, for different ranges Δ of noise fluctuation (markers: significant correlations, dashed lines: confidence interval obtained by shuffling, see Supplementary Materials and Methods).

tional elements are needed to accurately model the empirical UP-DOWN state dynamics during sleep.

Interplay between external fluctuation and adaptation strength

In order to investigate the mechanism entering into play during sleep we observe that, additionally to adaptation strength, another natural parameter for affecting UP-DOWN state durations is the amount of noise σ. Indeed, the higher the fluctuations in the system, the shorter the DOWN states and the longer the UP states (Fig. 2A), implying that UP state and DOWN state durations vary in

an anti-correlated fashion with σ. In other terms, if σ were to vary throughout time, a negative correlation could be observed between consecutive DOWN and UP state durations.

It is important to note, at this point, that our analyses are performed on relatively long recordings (from 20 minutes to several hours), and therefore one could assume that the properties of the system may change throughout the time of the recordings. The time scale T over which such changes occur seems relatively slow as compared to that of UP-DOWN dynamics ($\sim$ 1 s), i.e. in the range of tens of seconds.

To account for correlation inversion in our model, we introduce a parameter Δ describing the variability of noise amplitude σ throughout time. Here, the noise σ takes successive values within a range Δ of amplitudes σ (see Supplementary Materials and Methods), where each value is held constant over a time interval of duration T, as demonstrated in the inset of 2B. It should be noted that the resulting UP-DOWN correlations do not depend on the specific choice of T, as far as it is long enough to contain a sufficient number of UP-DOWN transitions in order to obtain well-defined UP DOWN statistics (in the plots shown in Fig 2 $T = 100$s).

By introducing variation of noise amplitude in time, a banana shape is observed in the scatter plot of UP and DOWN state duration, that disappears as the adaptation strength b is increased (Fig. 2B). Accordingly, a negative correlation between UP and DOWN state durations emerges increasing the range Δ of variation of the noise amplitude σ. Moreover, for sufficiently high Δ, an increase in the adaptation strength b is able to induce a transition from negative (sleep-like) to positive (anesthesia-like) correlation. In other words, adaptation is able to filter out noise variability, thus determining a positive correlation.

Apparent in the scatter plots of panel 2B, when adaptation is low, various values of noise amplitude σ (indicated by colors) cluster together in the scatter plot, altogether yielding a banana shape. Conversely, for high adaptation strength, data representing different values of noise amplitude overlap in the scatter plot, resulting in a non-significant or positive correlation. This can be understood as strong adaptation limiting the duration of UP states (green line in Fig. 2A, right), even in the presence of strong noise, and more generally controlling the transitions between UP and DOWN states. In sum, the model highlights the dominant mechanisms at work in each brain state, with the system being strongly adaptation driven in anesthesia, and fluctuation driven in sleep.

To investigate functional consequences of this difference in neuromodulation between sleep and anesthesia, we perform simulations to evaluate to what extent a stimulus affects collective dynamics. As shown in Fig. 3, the stimulus is simulated by delivering a spike train with Poisson statistics to all neurons, and the spike count after the stimulation is compared in the presence and in the absence of the stimulus (see Supplementary Materials and Methods). Immediately after the stimulation, anesthesia-like network is more responsive: as higher adaptation makes the network more silent, more spikes are evoked by the stimulus, relative to spontaneous firing rates. However, in the sleep-like net-

work the difference between stimulated and non-stimulated dynamics diverges significantly faster, as lower adaptation makes the dynamics more sensitive to a stimulus. After tens of seconds, we therefore find that the difference between stimulated and non-stimulated networks is larger for low adaptation, suggesting a longer memory of the stimulus in the sleep-like case. This confirms that low adaptation strength renders sleep-like networks more sensitive to external noise and stimulations, thus allowing more encoding and memory of external inputs than in anesthesia-like networks.

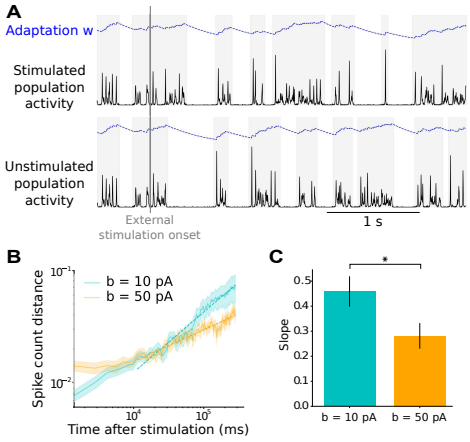

Fig. 3. Higher sensitivity to perturbations in sleep-like versus anesthesia-like networks (A) A stimulus is delivered during an UP state to all neurons in the network (upper panel) and the dynamics is compared to the system without stimulation (lower panel). (B) Absolute difference between population spike counts over time in stimulated and non-stimulated networks, normalised by non-stimulated mean spike count, for two values of adaptation strength b, averaged over trials (shaded area: error in the mean over all trials, see Supplementary Materials and Methods). (C) Linear regression slope for all trials, for the two different values of adaptation strength (error bars: error in the mean over all trials). The slope is significantly larger (independent Student's T-test, $p = 0.03$) for lower adaptation, denoting less stable dynamics and longer network memory in the sleep-like case.

Model prediction on non-stationarity in UP and DOWN state durations

A crucial ingredient of our model is the variability Δ in noise amplitude, especially in the sleep-like regime. Indeed, for lower adaptation strength, such as in SWS, noise fluctuations may play a larger role in shaping UP-DOWN dynamics. Accordingly, we expect to observe a higher variability in UP and DOWN state durations (as a direct outcome of noise variability, see Fig. 1) during sleep with

respect to anesthesia. Comparing the mean empirical values of UP and DOWN state durations over relatively long time windows of 100 UP-DOWN cycles (i.e. 10^2 s), we observe a higher variability, of the order of 200%, under sleep as compared to under anesthesia, as predicted by the model (see Supplementary Materials and Methods). To further characterize the time scale of noise fluctuations, the time window size was varied, and the correlations across windows were studied. By collecting UP and DOWN durations in each window during sleep, we observe that, just as in our model, UP-DOWN state durations belonging to different windows have different correlation values. For short time windows (up to the order of 50 cycles), the Pearson coefficient is positive in the majority of windows, but becomes negative when computed over longer windows (see Supplementary Material). This suggests that fluctuations take place at a time scale T that can be as fast as the order of 10 seconds.

It can be noted this confirms the previous assumption that the time scale T of fluctuations is longer than the UP-DOWN cycle duration (of the order of 1 second). Conversely, T is much shorter than the duration of all our recordings (12 minutes to 3 hours) for either sleep or anesthesia, such that the absence of a negative correlation during anesthesia cannot be explained by too short recordings (unless T in anesthesia is not the same as in sleep, but much longer than the duration of the recordings studied here).

Additionally, the presence of background fluctuations at time scale T during sleep and not anesthesia is consistent with the apparent long memory of the UP-DOWN state duration correlation in SWS. Indeed, one may consider a period of time T over which background noise may be approximated as constant. During that period, if noise amplitude is high, UP states are long, and DOWN states short, and conversely if noise amplitude is low. Then whatever the lag, UP state durations are negatively correlated to the durations of DOWN states before or after them, provided that they occur within the same period of duration T. It is verified that the order of magnitude of T matches that of the time scale of the memory in sleep (a few UP-DOWN cycles, Fig. 1C, F, I).

Effect of *in vitro* modulation of adaptation strength on UP/DOWN correlation

Another strong prediction of our model is the ability of adaptation strength to modulate the correlations in UP and DOWN state durations. Spike-frequency adaptation models an effective action of activity-dependent potassium conductances, physiologically affected by neuromodulators [16].

It has been observed that neuromodulation is depressed during anesthesia [14], and thus the strength of adaptation should be increased [16]. This is consistent with our model prediction, where a transition to anesthesia (higher adaptation) yields a positive correlation between UP and DOWN states.

Nevertheless, a more direct experiment is preferable in order to validate our prediction. To this purpose we performed extracellular recordings of neural activity in acute slices of entorhinal cortex from wild type juvenile mice.

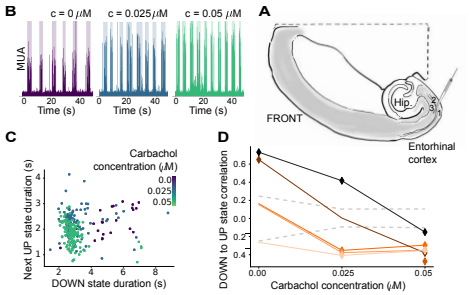

Fig. 4. Blocking adaptation by addition of carbachol in mouse slice preparations produces a transition from anesthesia-like to sleep-like dynamics (A) Illustration of a horizontal mouse brain slice. Extracellular recording pipettes for Multi-Unit Activity (MUA) were placed in layer 2/3 of the entorhinal cortex. (B) MUA throughout time, recorded for different carbachol concentrations c for an example slice (shaded: UP state detection). UP state frequency is observed to increase with carbachol concentration. (C) For the same example slice, UP state against previous DOWN state duration for different carbachol concentrations, showing a positive correlation (r = 0.64, p ¡ 0.05) in the control condition ($c = 0\mu M$), non-correlated for an intermediary concentration ($c = 0.025\mu M$, r = 0.00), and a negative correlation ($c = 0.05\mu M$, r = -0.37, p ¡ 0.05) when the highest carbachol concentration is added. (D) For all recorded slices, correlation between UP state and previous DOWN state duration as a function of carbachol concentration. Consistent with model predictions on the effect of adaptation strength, all slices exhibit a positive or non-significant, 'anesthesia-like' correlation in the control condition ($c = 0\mu M$) and a negative, 'sleep-like' correlation for the highest carbachol concentration ($c = 0.05\mu M$), when adaptation is blocked (markers: significant correlations, colors: different slices, dashed lines: shuffles, see Supplementary Materials and Methods).

In control conditions, a certain variability was observed in both UP and DOWN state duration, sufficient to measure UP-DOWN states duration correlation.

The great advantage of *in vitro* preparations is the possibility to pharmacologically modulate adaptation [16] by dissolving neuromodulators in the artificial cerebrospinal fluid (ACSF) in which the slice is recorded.

To stimulate an effective decrease of adaptation strength, carbachol, an agonist of both nicotinic and muscarinic acetylcholine (ACh) receptors is used [16].

By increasing concentrations of carbachol (0, 0.025, 0.05 μM), we observe lengthening UP states and shortening DOWN states, Fig. 4, in accordance with a lower amount of spike-frequency adaptation, as in the model.

Finally, we report a clear tendency to more negatively correlated, sleep-like UP and DOWN states durations at higher carbachol concentrations. This confirms the predictions of our model, where an increase of adaptation strength permits a more positive correlation between UP and DOWN states durations.

3 Discussion

In the present paper, we have shown two types of slow waves by analyzing multi-electrode extracellular recordings in human and animal cerebral cortex. This conclusion was reached based on the temporal patterns of UP and DOWN states, an alternation of which causes slow waves to emerge. A first type of slow waves shows positively correlated consecutive UP and DOWN states, such as that found in previous work [11], while we find a second type of slow wave displaying negatively correlated consecutive UP and DOWN states. The first type of slow waves is seen during natural slow-wave sleep, while the second type appears to prevail in anesthetized states. Using computational models, we show that different levels of adaptation can explain the two different types of slow-waves. This prediction was tested in cortical slices, where the level of adaptation can be modulated by cholinergic agonists. These experiments demonstrate a cholinergic switch between the two types of slow waves. We also find that the two types of slow waves differ in their sensitivity to external inputs. We discuss below the significance of these findings, and perspectives for future work.

The difference between slow-wave sleep and anesthesia was robust across several species and brain regions. These results hold for slow waves produced by two different anesthetics, in contrast to natural slow waves observed in sleep. A larger effect of noise fluctuations throughout time on the network dynamics is observed during sleep, yielding a negative, long-memory correlation between UP and DOWN state durations. Conversely, during anesthesia the dynamics is more stable and characterized by short-memory and positive correlation between state durations. Employing a spiking neuron network model revealed that during anesthesia such noise fluctuations produce much smaller effects on population dynamics, as the fluctuations are filtered out by a strong modulatory effect (e.g. spike-frequency adaptation, which is controlled by acetylcholine levels). For the sake of simplicity, external noise was chosen to be the only effective

source of variability in the model. Nevertheless, this is not the only possible choice: one could also consider variability in other parameters in time, that can be tuned to produce longer UP states and shorter DOWN states, like inhibitory conductance [23] or even adaptation strength (Fig. 4E). In sum, adaptation filters out time variation in the system's parameters, in anesthesia but not in sleep. This mechanism is confirmed by modulation of spike-frequency adaptation strength in acute cortical slices. Indeed, addition of charbachol, a cholinergic receptor agonist, induced a switch between anesthesia-like and sleep-like slow-waves.

In addition, we show the implications of a switch in slow wave type for the network's coding properties, with sleep-like slow waves associated with higher sensitivity to stimuli and greater capacity for network memory. This may help explain why key cognitive processes, such as memory consolidation, can take place during sleep [2–4], while anesthesia causes amnesia and memory impairment [24–26]. Our observation of two types of slow-waves suggests that slow-wave dynamics may be important to explain these differences. For example for memory consolidation to occur, the cortex should encode information by changing its dynamics upon receiving signals from the hippocampus. This implies that a non-trivial change in external input should be able to modulate the statistics of cortical activity. We showed (Fig. 3) that in anesthesia, unlike in sleep, strong adaptation filters out the effects of external perturbations on UP-DOWN state dynamics, so that any information encoded in the amplitude of inputs to the neural assembly does not affect the network dynamics, and consequently will not be encoded.

Finally, we emphasize that understanding the role of adaptation in filtering out external variability may shed light on pathological conditions where adaptation is disturbed. For example, the cholinergic system, that modulates spike-frequency adaptation [16], breaks down in Alzheimer's disease [27]. A slowing down of slow oscillatory patterns during SWS [28, 29] and a loss of memory [30] are also biomarkers of the disease. With loss of acetylcholine, spike-frequency adaptation will be increased, similarly to under anesthesia, and it is conceivable that the cortex of Alzheimer's patients cannot encode fluctuating inputs from the hippocampus during sleep due to anesthesia-like slow-wave dynamics. This mechanism may contribute to explaining why new memories cannot be formed, and to better comprehending how treatments restoring acetylcholine levels alleviate Alzheimer's sleep and memory symptoms [31]. Our study directly predicts that the anesthesia-type slow-wave dynamics should be observed in Alzheimer's patients during their natural sleep, and provides an approach to modulating and quantifying the restoration of sleep type slow waves, perhaps a fruitful direction to explore in the design of new therapies.

4 Acknowledgments

This project/research has received funding from the European Unions Horizon 2020 Framework Programme for Research and Innovation under Grant Agreements No. 720270 (Human Brain Project SGA1) and No. 785907 (Human Brain

Project SGA2). The authors thank C. Desbois, Z. Gironés, M. Mattia, V. Medel, M.V. Sanchez-Vives, and Y. Zerlaut for useful discussion.

4.1 Citations

References

1. Steriade M, Contreras D, Dossi RC, Nunez A (1993) The slow (<1 hz) oscillation in reticular thalamic and thalamocortical neurons: scenario of sleep rhythm generation in interacting thalamic and neocortical networks. *Journal of Neuroscience* 13(8):3284–3299.
2. Wilson MA, McNaughton BL (1994) Reactivation of hippocampal ensemble memories during sleep. *Science* 265(5172):676–679.
3. Mehta MR (2007) Cortico-hippocampal interaction during up-down states and memory consolidation. *Nature neuroscience* 10(1):13.
4. Peyrache A, Khamassi M, Benchenane K, Wiener SI, Battaglia FP (2009) Replay of rule-learning related neural patterns in the prefrontal cortex during sleep. *Nature neuroscience* 12(7):919.
5. Battaglia FP, Sutherland GR, McNaughton BL (2004) Hippocampal sharp wave bursts coincide with neocortical "up-state" transitions. *Learning & Memory* 11(6):697–704.
6. Brown EN, Lydic R, Schiff ND (2010) General anesthesia, sleep, and coma. *New England Journal of Medicine* 363(27):2638–2650.
7. Akeju O, Brown EN (2017) Neural oscillations demonstrate that general anesthesia and sedative states are neurophysiologically distinct from sleep. *Current opinion in neurobiology* 44:178–185.
8. Niedermeyer E, Sherman DL, Geocadin RJ, Hansen HC, Hanley DF (1999) The burst-suppression electroencephalogram. *Clinical Electroencephalography* 30(3):99–105.
9. Bruhn J, Röpcke H, Rehberg B, Bouillon T, Hoeft A (2000) Electroencephalogram approximate entropy correctly classifies the occurrence of burst suppression pattern as increasing anesthetic drug effect. *Anesthesiology: The Journal of the American Society of Anesthesiologists* 93(4):981–985.
10. Deco G, Martí D, Ledberg A, Reig R, Vives MVS (2009) Effective reduced diffusion-models: a data driven approach to the analysis of neuronal dynamics. *PLoS computational biology* 5(12):e1000587.
11. Jercog D, et al. (2017) Up-down cortical dynamics reflect state transitions in a bistable network. *Elife* 6:e22425.
12. Tort-Colet N, Capone C, Sanchez-Vives M, Mattia M (2018) Attractor dynamics of cortical assemblies underlying the transition from deep to light anesthesia. in *Barcelona Computational, Cognitive and Systems Neuroscience*. (Barcelona, Spain).
13. Sanchez-Vives MV, McCormick DA (2000) Cellular and network mechanisms of rhythmic recurrent activity in neocortex. *Nature neuroscience* 3(10):1027.
14. Jones BE (2003) Arousal systems. *Front Biosci* 8(5):438–51.
15. McCormick DA (1992) Neurotransmitter actions in the thalamus and cerebral cortex and their role in neuromodulation of thalamocortical activity. *Progress in neurobiology* 39(4):337–388.

16. McCormick DA, Williamson A (1989) Convergence and divergence of neurotransmitter action in human cerebral cortex. *Proceedings of the National Academy of Sciences* 86(20):8098–8102.
17. Compte A, Sanchez-Vives MV, McCormick DA, Wang XJ (2003) Cellular and network mechanisms of slow oscillatory activity (¡ 1 hz) and wave propagations in a cortical network model. *Journal of neurophysiology* 89(5):2707–2725.
18. Mattia M, Sanchez-Vives MV (2012) Exploring the spectrum of dynamical regimes and timescales in spontaneous cortical activity. *Cognitive neurodynamics* 6(3):239–250.
19. Capone C, et al. (2017) Slow waves in cortical slices: how spontaneous activity is shaped by laminar structure. *Cerebral Cortex* pp. 1–17.
20. Brette R, Gerstner W (2005) Adaptive exponential integrate-and-fire model as an effective description of neuronal activity. *Journal of neurophysiology* 94(5):3637–3642.
21. Pospischil M, et al. (2008) Minimal hodgkin–huxley type models for different classes of cortical and thalamic neurons. *Biological cybernetics* 99(4-5):427–441.
22. Holcman D, Tsodyks M (2006) The emergence of up and down states in cortical networks. *PLoS computational biology* 2(3):e23.
23. Sanchez-Vives MV, et al. (2010) Inhibitory modulation of cortical up states. *Journal of neurophysiology* 104(3):1314–1324.
24. Culley DJ, Baxter M, Yukhananov R, Crosby G (2003) The memory effects of general anesthesia persist for weeks in young and aged rats. *Anesthesia & Analgesia* 96(4):1004–1009.
25. Rudolph U, Antkowiak B (2004) Molecular and neuronal substrates for general anaesthetics. *Nature Reviews Neuroscience* 5(9):709.
26. Timofeev I, Chauvette S (2018) Sleep, anesthesia, and plasticity. *Neuron* 97(6):1200–1202.
27. Kihara T, Shimohama S (2004) Alzheimer's disease and acetylcholine receptors. *Acta neurobiologiae experimentalis* 64(1):99–106.
28. Mander BA, Winer JR, Jagust WJ, Walker MP (2016) Sleep: a novel mechanistic pathway, biomarker, and treatment target in the pathology of alzheimer's disease? *Trends in neurosciences* 39(8):552–566.
29. Castano-Prat P, Perez-Zabalza M, Perez-Mendez L, Escorihuela RM, Sanchez-Vives MV (2017) Slow and fast neocortical oscillations in the senescence-accelerated mouse model samp8. *Frontiers in aging neuroscience* 9:141.
30. Prinz PN, et al. (1982) Sleep, eeg and mental function changes in senile dementia of the alzheimer's type. *Neurobiology of aging* 3(4):361–370.
31. Babiloni C, et al. (2013) Effects of acetylcholinesterase inhibitors and memantine on resting-state electroencephalographic rhythms in alzheimer's disease patients. *Clinical Neurophysiology* 124(5):837–850.
32. Peyrache A, et al. (2012) Spatiotemporal dynamics of neocortical excitation and inhibition during human sleep. *Proceedings of the National Academy of Sciences* 109(5):1731–1736.
33. Dehghani N, et al. (2016) Dynamic balance of excitation and inhibition in human and monkey neocortex. *Scientific reports* 6:23176.
34. Teleńczuk B, et al. (2017) Local field potentials primarily reflect inhibitory neuron activity in human and monkey cortex. *Scientific reports* 7:40211.
35. Le Van Quyen M, et al. (2016) High-frequency oscillations in human and monkey neocortex during the wake–sleep cycle. *Proceedings of the National Academy of Sciences* 113(33):9363–9368.

36. Nghiem TA, Telenczuk B, Marre O, Destexhe A, Ferrari U (2018) Maximum-entropy models reveal the excitatory and inhibitory correlation structures in cortical neuronal activity. *Physical Review E* 98(1):012402.
37. Benchenane K, et al. (2010) Coherent theta oscillations and reorganization of spike timing in the hippocampal-prefrontal network upon learning. *Neuron* 66(6):921–936.
38. Tavoni G, Ferrari U, Battaglia FP, Cocco S, Monasson R (2017) Functional coupling networks inferred from prefrontal cortex activity show experience-related effective plasticity. *Network Neuroscience* 1(3):275–301.
39. Kadir SN, Goodman DF, Harris KD (2014) High-dimensional cluster analysis with the masked em algorithm. *Neural computation* 26(11):2379–2394.
40. Kohn A, Smith M (2016) Utah array extracellular recordings of spontaneous and visually evoked activity from anesthetized macaque primary visual cortex (v1).
41. Smith MA, Kohn A (2008) Spatial and temporal scales of neuronal correlation in primary visual cortex. *Journal of Neuroscience* 28(48):12591–12603.
42. Paxinos G, Watson C (2004) *The rat brain in stereotaxic coordinates*. (Elsevier Academic, London).
43. Reig R, Mattia M, Compte A, Belmonte C, Sanchez-Vives MV (2010) Temperature modulation of slow and fast cortical rhythms. *Journal of neurophysiology* 103(3):1253–1261.
44. Ruiz-Mejias M, Ciria-Suarez L, Mattia M, Sanchez-Vives M (2011) Slow and fast rhythms generated in the cerebral cortex of the anesthetized mouse. *J Neurophysiol* 106(6):2910–2921.
45. Mattia M, Perez-Zabalza M, TORT-COLET N, Sanchez-Vives M (2016) Metastable dynamics underlying the multiscale organization of slow oscillations. in *Society for Neuroscience*. (San Diego, California).
46. Tahvildari B, Wölfel M, Duque A, McCormick DA (2012) Selective functional interactions between excitatory and inhibitory cortical neurons and differential contribution to persistent activity of the slow oscillation. *Journal of Neuroscience* 32(35):12165–12179.
47. Sadoc G (2014) Elphy software.
48. Destexhe A (2009) Self-sustained asynchronous irregular states and up–down states in thalamic, cortical and thalamocortical networks of nonlinear integrate-and-fire neurons. *Journal of computational neuroscience* 27(3):493.
49. Renart A, et al. (2010) The asynchronous state in cortical circuits. *science* 327(5965):587–590.
50. Tort-Colet N, Capone C, Mattia M, M.V. SV, Destexhe A (2018) Bimodality of cortical up states and thalamic modulation of up state duration: an experimental and computational study. in *Barcelona Computational, Cognitive and Systems Neuroscience*. (Barcelona, Spain).

5 Supplementary Information

Neural recordings

Human temporal cortex in deep sleep The data was recorded with intracranial multi-electrode array recordings of 92 neurons in the temporal cortex of an epileptic patient, the same data-set used by [32–36]. The record of interest spans across approximately 12 hours, including periods of wakefulness as well as

several stages of sleep. Recordings were performed in layer II/III of the middle temporal gyrus, in an epileptic patient (found to be far from the epileptic focus and not registering epileptic activity outside of generalized seizures). Data acquisition in that region was enabled by implanting a multi-electrode array, of dimensions 1 mm in thickness and 4x4 mm in area, with 96 micro-electrodes separated by 400 μm spacings. The array was implanted to localize seizure foci. A 30-kHz sampling frequency was employed for recording. Switches in brain state (wakefulness, SWS, REM, seizure, ...) throughout the recording were noted from the patient's behavioural and physiological parameters, yielding one hour of SWS on which our analyses were focused. Using spike sorting methods on the obtained data, 92 neurons have been identified. Analysis of the spike waveforms for each of these neurons allowed their classification as putative excitatory (E) and inhibitory (I) neurons. Using the spike times of each neuron, cross-correlograms for all pairs of neurons were also computed to determine whether each neuron's spikes had an excitatory (positive correlation) or an inhibitory (negative correlation) effect on other neurons through putative monosynaptic connections. It should be noted that neurons found to be excitatory exactly corresponded to those classified as regular spiking (RS), while all inhibitory neurons were also fast spiking (FS). We only retained neurons spiking throughout the recording for our analyses, amounting to 71 neurons of which 21 were I neurons. Spikes were binned into 1 ms wide time bins for all subsequent analyses. A statistical analysis of UP DOWN states duration is presented in Fig.SS1 (panels A-D and E left).

Monkey premotor cortex in deep sleep Spiking activity (the same dataset as used in [33–36]) in layer III/IV of the premotor cortex of a macaque monkey was recorded by multi-electrode arrays throughout a night. A 10-kHz sampling frequency was employed for recording. Classification of brain states, for extraction of SWS periods, was performed by visual inspection of the Local Field Potential (LFP), over time periods of 5 s, by identifying as SWS periods presenting large-amplitude oscillations in the 1-2 Hz frequency range [36], of which 141 spiked throughout the whole recording, yielding three hours of SWS data for subsequent analyses. All analyses in this work were performed with spikes binned into 1 ms time bins.

Rat prefrontal cortex in deep sleep The analysis was performed on the dataset of single unit activities previously employed in [4,37,38]. Here we provide a short description only. Five Long-Evans male rats were chronically implanted with tetrodes in the prelimbic subdivision of the medial prefrontal cortex and in the intermediate-ventral hippocampus. Tetrodes in the hippocampus were used for identification of non-REM sleep periods, through a clustering analysis of the LFP power within the cortical delta band ($1-4Hz$), hippocampal theta ($5-10Hz$) and cortical spindles ($10-20Hz$) together with estimates of the speed of head movements. Tetrodes in the cortex were used for single unit recording. Spike sorting has been performed using *KlustaKwik* [39]. Recordings were organized

in daily sessions, where the rat undergoes a first sleeping epoch, then a task learning epoch, in which the rat performs an attentional set shift task on a Y shaped maze, and finally a second sleeping epoch, each epoch lasting 30 mins. In general, the neurons recorded differed from a session to another, with the number of cells recorded per session varying between 10 and 50. For the analysis of up/down state duration, the results from all session from the same rat were joined together, but pre-task and post-task sleep were kept separated.

Monkey primary visual cortex in sufentanil anesthesia The data-set may be found at [40], as described in [41]. Four adult macaque monkeys were recorded using a total of six multielectrode arrays implanted in the primary visual cortex. Sufentanil (4-18 μg/kg/hr) was used for anesthesia. Recordings were obtained while animals viewed a uniform gray screen, over periods of between 20 and 30 minutes long. Spontaneous spiking activity from 70 100 neurons was recorded and spike-sorted for each array. Spikes were binned into 1 ms time bins for subsequent analyses. A statistical analysis of UP DOWN states duration is presented in Fig.1E right.

Rat primary visual cortex in ketamine anesthesia 7 adult male Wistar rats weighting 211 58 g (mean s.d.) were anesthetized via intraperitoneal injection of ketamine (120 mg/kg) and medetomidine (0.5 mg/kg). Atropine (0.05 mg/kg) was injected subcutaneously to prevent respiratory secretions. Rectal temperature was maintained at 37C. A craniotomy was performed to access the primary visual (V1) cortex (7.3 mm AP, 3.5 mm ML) of the right hemisphere [42].

Recordings of cortical activity under anesthesia were obtained with a 16-channel silicon probe (1 shank with 16 linearly spaced sites at $100\mu m$ increments with impedances of $0.6 - 1M\Omega$ at 1kHz (NeuroNexus Technologies, Ann Arbor, MI)) introduced perpendicularly in V1 under visual guidance until the most superficial recording site was aligned with the cortical surface. Signals were amplified (Multi Channel Systems), digitized at 10kHz and acquired with a CED acquisition board and Spike 2 software (Cambridge Electronic Design, UK). Recordings had an average length of 951.46 +/-219.30 seconds. UP and DOWN states were singled out by thresholding the multi-unit activity (MUA), which was estimated as the power of the Fourier components at high frequencies (200-1500 Hz) of the extracellular recordings (LFP) [12, 23, 43–45]. For each experiment, we selected the channel with maximum MUA during the Up state, whose location in depth corresponds to cortical layer 5 [12, 45].

All experiments were supervised and approved by the local Ethics Committee and were carried out in accordance with the present laws of animal care, EU guidelines on protection of vertebrates used for experimentation (Strasbourg 3/18/1986) and the local law of animal care established by the Generalitat of Catalonia (Decree 214/97, 20 July).

Mouse entorhinal cortex slice preparations We prepared brain slices exhibiting spontaneous slow waves in entorhinal cortex using a method described in [46]. The mice were of wild-type (C57BL/6J) and 11-18 days old.

The dissection and slice cutting were performed in an ice-cold cutting solution containing (in mM): 85 NaCl, 75 sucrose, 3 KCl, 26 $NaHCO_3$, 1.25 NaH_2PO_4, 3.5 $MgSO_4$, 0.5 $CaCl_2$, 10 glucose, 3 myo-inositol, 3 Na-pyruvate, 0.5 L-ascorbic acid and aerated with 95% O_2 and 5% CO_2. Lower concentrations of Na^+ and Ca^{2+}, and a higher concentration of Mg^{2+} in the cutting solution, compared to a standard ACSF, are applied to minimize neuronal damage during cutting.

We cut slices at a 15° angle off the horizontal plane with the thickness of 310 μm. After cutting, slices were placed in a cutting solution at temperature of 35° C for 30 min.

The slices were then kept at room temperature in a storing solution containing (in mM): 126 NaCl, 3 KCl, 26 $NaHCO_3$, 1.25 NaH_2PO_4, 2 $MgSO_4$, 2 $CaCl_2$, 10 glucose, 3 myo-inositol, 3 Na-pyruvate, 0.5 L-ascorbic acid.

For recording, the slices were transfered to a submersion chamber and placed between nylon nets. The well oxygenated recording solution was flowing with the speed of 4ml/min. The recording solution was similar to storing solution, with only $CaCl_2$ and $MgSO_4$ concentrations reduced to 1.2 and 1 mM respectively. The extracellular field was recorded with glass electrodes with a resistance of 2-3 $M\Omega$. The electrode was placed in layer 2/3 of the entorhinal cortex.

Electrophysiological data was acquired using the ELPHY software [47]. The multi-unit activity was obtained from the signal by calculating the time-averaged power of the signal in the frequency range (0.3 - 2 kHz).

Spiking network model

We consider a population of $N = 10^4$ neurons connected over a random directed network with probability of connection $p = 5\%$. We consider excitatory and inhibitory neurons, with 20% inhibitory neurons. The dynamics of each of the two types of neurons is based on the adaptive integrate and fire model, described by the following equations

$$c_m \frac{dv_i}{dt} = g_L(E_L - v_i) + g_L k_a e^{\frac{v_i - v_{thr}}{k_a}} - w_i + I_{syn} + \sigma\xi_i(t) \tag{1}$$

$$\frac{dw_i}{dt} = -\frac{w_i}{\tau_w} + b \sum_{t_{sp}(i)} \delta(t - t_{sp}(i)) + a(v_i - E_L), \tag{2}$$

where c_m is the membrane capacity, v_i is the voltage of neuron i and whenever $v_i > v_{thr}$ at time $t_{sp}(i)$, v_i is reset to the resting voltage v_{rest} and fixed to that value for a refractory time τ_r. The exponential term mimics activation of sodium channels and parameter k_a describes its sharpness. Inhibitory neurons are modeled according to physiological insights [48] as fast spiking FS neurons with no adaptation while the strength b of spike-frequency adaptation in excitatory regular spiking RS neurons is varied. The synaptic current I_{syn} received by

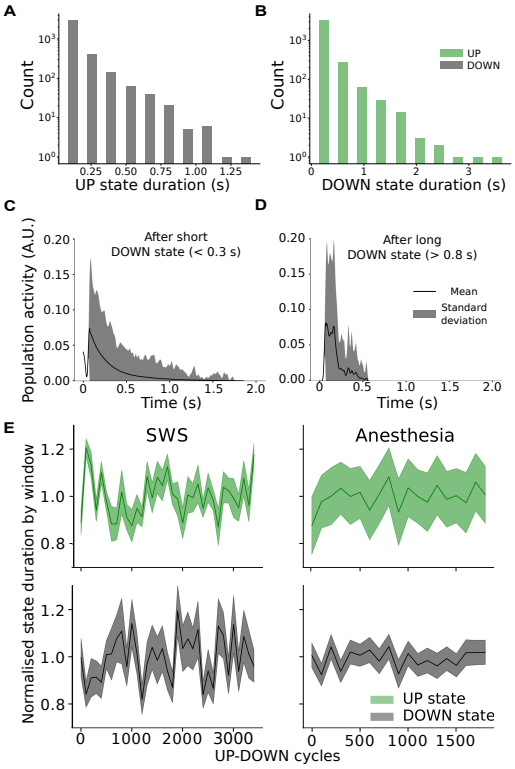

Fig. S1. UP DOWN states statistics in experimental data (A-B) Both UP and DOWN state durations follow exponential long-tailed, distributions. (C-D) Averaged population firing rate, aligned to UP state onset, after short (C) or long (D) DOWN state durations. UP states following very long DOWN states, $> 0.8s$, are always short, while UP states following the shortest DOWN states, $< 0.3s$, can be up to around three times longer. (E) Mean UP and DOWN state durations in 100 UP-DOWN-cycle windows in time, normalized by the mean duration over the whole recording, highlight larger fluctuations across windows in sleep (human data, left) than anesthesia (rat data, right). The mean in each window is represented by a full line, while the standard error in the mean is represented by the shaded area.

neuron i is the result of the spiking activity of all pre-synaptic neurons $j \in \text{pre}(i)$ of neuron i. This current can be decomposed in the result received from excitatory E and inhibitory I pre-synaptic spikes $I_{syn} = (E_e - v_i)I^e_{syn} + (E_I - v_i)I^I_{syn}$. Notice that we consider voltage dependent conductances. Finally, we model I^x_{syn} as a decaying exponential function that takes kicks of amount Q_x at each pre-synaptic spike, i.e.:

$$I^x_{syn}(t) = Q_x \sum_{exc.pre} \delta(t - t^x_{sp}(i)) e^{-\frac{t - t^x_{sp}(i)}{\tau_x}}, \tag{3}$$

where x represents the population type ($x = E, I$), τ_x is the synaptic decay time scale and Q_x the quantal conductance. We will have the same equation with $E \to I$ for inhibitory neurons. Every neuron i receives an identically distributed white noise $\xi(t)$ of zero mean and instantaneously decaying autocorrelation $\langle \xi_i \rangle = 0$, $\langle \xi_i(t)\xi_j(t+s)\rangle = \delta_{i,j}\delta(t-s)$. The noise amplitude σ is a piecewise constant function of time, i.e. its value stays constant for a time window of length T and is extracted from a uniform distribution of amplitude Δ. In our simulations Δ varies and we use $T = 100$s, in accordance to the observed variability of UP-DOWN states duration during sleep.

A transient of 1s after simulation onset is discarded from all analyses. An example of the dynamics of this system is reported in Fig.S2A and statistics of UP DOWN states durations obtained with the model are shown in Fig.S2B-E.

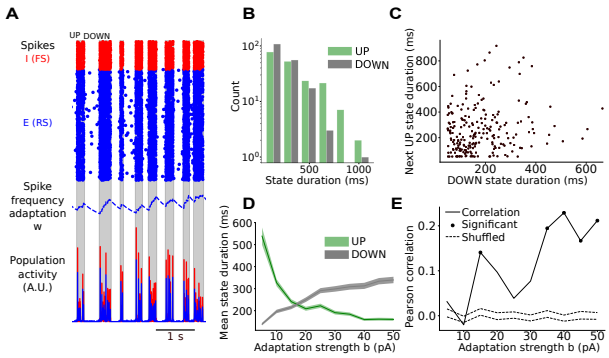

Fig. S2. UP and DOWN states in computational model (A) Spikes and population activity produced by a spiking model of RS (blue)-FS (red) neuron network with spike-frequency adaptation on RS cells (blue, dashed line) exhibits UP-DOWN state dynamics (grayed: UP state detection). (B) UP and DOWN state durations are exponentially distributed, consistently with empirical data in both sleep and anesthesia. (C) UP state against previous DOWN state durations yield a significant positive correlation ($r = 0.16$, $p < 0.05$) in this example simulation. (D) State durations in different simulations with increasing adaptation strength, showing shortening UP states and lengthening DOWN states (full line: mean, shaded area: standard error in mean). (E) Modeled UP to previous DOWN state duration correlation against adaptation strength reveals systematic positive or non-significant correlations and indicates an increase of the correlation with adaptation level (markers: significant correlations, shaded: interval of confidence obtained by shuffling). This is therefore a good model for anesthesia, but not deep sleep.

To deliver a stimulus to the network, each neuron receives an external Poissonian spike train of frequency 0.05 Hz for a duration of 50 ms. Stimuli are delivered halfway through the first UP state after the discarded transient. To directly compare network dynamics in the presence and absence of a stimulus, the network connectivity matrix and initial conditions are the same in both simula-

Table 1. Model parameters

Neuron type	Parameter name	Symbol	value
RS & FS	Membrane Capacity	C_m	150pF
RS & FS	Leakage Conductance	g_L	10nS
RS & FS	Excitatory quantal conductance	Q_E	1nS
RS & FS	Inhibitory quantal conductance	Q_I	5nS
RS & FS	Spiking threshold	v_{thr}	-50mV
RS & FS	Resting voltage	v_{rest}	-65mV
RS & FS	Excitatory synapses time decay	τ_E	5ms
RS & FS	Inhibitory synapses time decay	τ_I	5ms
RS & FS	Refractory time	τ_r	5ms
RS	Sodium sharpness	k_a	2mV
RS	Leakage reversal	E_L	-60mV
RS	adaptation current increment	b	varies
RS	adaptation conductance	a	0nS
RS	adaptation time constant	τ_w	500ms
FS	Sodium sharpness	k_a	0.5mV
FS	Leakage reversal	E_L	-65mV
FS	adaptation current increment	b	0nS
FS	adaptation conductance	a	0nS

tions, such that dynamics before the stimulus onset are identical, and differences in dynamics following the onset are only due to the stimulation. The cumulative spike count is computed in each case, at each point in time. The normalized distance between the spike counts with and without stimulus is defined by:

$$D = \frac{|s' - s|}{< s >}, \tag{4}$$

where s is the spike count for the unstimulated network, s' is the spike count for the stimulated network, and $< \cdot >$ denotes time averaging. Each simulation lasts 30s, and the procedure is repeated 50 times, each time with different connectivity realization and initial condition set. In Fig. 3 of the main paper we report the average value of D over different realizations, together with its standard deviation.

Measures and UP DOWN states detection

The method to detect UP states ([49], Section 1.3.3. of Suppl Mat.) considers the sum of all cells' spike trains (bin size of 1 ms), $K(t) = \sum_i \sigma_i(t)$. The instantaneous population activity $m(t)$ is the smoothed $K(t)$, by convolution with a Gaussian density with width $\alpha = 10$ ms. Any period of time for which the instantaneous population activity
$m(t) > \theta \max(m(t))$ is considered an UP state, where the threshold θ was chosen in terms of the sparseness and non-stationarity of each data-set ($\theta = 0.2$ for most data-sets, as in [49], except human SWS and the spiking model, where $\theta = 0.02$,

and slice preparations, for which $\theta = 0.5$.). States lasting less than 50 ms were excluded by considering it a part of the previous sufficiently long state. States longer than 5 s are discarded from the analysis. Parameters used for detection were determined by visual inspection of the detection quality. It was also verified that slight variation of these parameters did not qualitatively affect the results presented in this work.

This method was tested against a different method where UP and DOWN states were singled out by setting a minimum state duration of 80ms and a threshold in log(MUA) values at 1/3 of the interval between the peaks of the bimodal distribution of log(MUA) corresponding to the Up and Down states. The algorithm, adapted from [12, 18, 44, 50], yielded qualitatively identical results.

The Pearson correlation was then employed to evaluate how strong and significant the correlation between UP state and previous DOWN state durations are. As a further test for significance, the information present in time structure was destroyed by shuffling all DOWN state durations, while leaving UP state durations in their empirical order, and computing the Pearson correlation again. This procedure is repeated 1,000 times, and the mean and standard deviation of the Pearson correlations obtained each time are calculated. The interval contained within two standard deviations above and below the mean of correlations obtained from shuffled is considered as a confidence interval. Indeed, a correlation well outside of this interval is highly unlikely to have been produced by a chance arrangement of UP and DOWN states in time, given the empirical distribution of their durations, and implies a non-trivial structure in time.

This procedure is used to evaluate the correlation between each UP state and the DOWN states surrounding it, $C(D_{n+k}, U_n)$, with $k = 0$ denoting the previous DOWN state to the considered UP state, negative k denoting previous DOWN states more distant in time, and positive k denoting DOWN states following the UP state of interest.